Green Chemistry



PAPER View Article Online
View Journal | View Issue



Cite this: *Green Chem.*, 2025, **27**, 793

Continuous-flow chemo-enzymatic gram-scale synthesis of indole-3-acetic acid†

In this work, a chemo-enzymatic reaction was developed to synthesize indole-3-acetic acid (IAA) in a continuous flow mode. The cascade reaction consists of the oxidative decarboxylation of L-tryptophan catalyzed by tryptophan 2-monooxygenase (TMO) and the subsequent acid-catalyzed hydrolysis. The telescoped continuous-flow reaction setup was systematically designed using design equations with empirical reaction kinetics, showcasing a flow biocatalytic development framework. Optimal conditions were selected to minimize byproducts from non-specific hydrolysis. This process gave a promising space-time yield (STY) of 11.16 g L^{-1} day⁻¹ while maintaining a high overall yield of 48.50%. This work demonstrates the feasibility of combining conventional chemical and enzymatic reactions, leveraging the strengths of both methods to enhance productivity and efficiency.

Received 17th October 2024, Accepted 6th December 2024 DOI: 10.1039/d4gc05236f

rsc.li/greenchem

Introduction

Indole-3-acetic acid (IAA, 1), one of the plant hormones in the auxin class, regulates plant cell elongation, tissue differentiation, and root promotion.^{1–3} The compound has been widely used in the agricultural field as a plant growth regulator (PGR) to promote crop production; in recent times, the applications of IAA and its derivatives are currently receiving attention in the pharmaceutical and medicinal fields owing to its scaffold sharing with other bioactive compounds potentially functioning as drugs⁴ (Fig. 1).

IAA was proposed to serve as a precursor to synthesize indole acetic acid sulfonate derivatives, (2) which potentially possess anti-cancer activity (as ecto-nucleotidase inhibitors).⁵ The coupling reactions of IAA derivatives were used in the synthetic route of Arcyriaflavin A (3) possessing indolocarbazole alkaloids' activities.⁶ Half reduction of IAA provides indole-3-acetaldehyde (IAAId, 4), which could be a precursor to des-

chloro 12-epi-fischerindole W nitrile (5) synthesis. The chemi-

All of these have led to a significant increase in global demand for the compound in several fields shown by its global market size of 26 million USD in 2024. The size of the market was also projected to reach 36 million USD in 2030 with a compound annual growth rate (CAGR) of 5.3%, globally. Thus, an increase in IAA manufacturing is required to serve the growing global demand for IAA.

IAA is naturally produced by plants¹⁴ and microorganisms engaged in plant–microbe interactions.^{15,16,17} Six metabolic pathways are reported to synthesize IAA, which could be classified based on their intermediates: the indole-3-acetamide (IAM) pathway, indole-3-pyruvic acid (IPyA) pathway, tryptamine (TAM) pathway, indole-3-acetonitrile (IAN) pathway, tryptophan side chain oxidase (TSO) pathway, and non-Trp-dependent pathway.¹⁸ These led to the use of whole-cell biocatalysis and fermentation primarily for IAA production, utilizing either native-host bioconversions or metabolic engineering approaches. New strains of microbes have been explored to enhance IAA productivity. Plant-growth-promoting yeasts (e.g., Candida spp., Pichia spp., and Tortispora spp.¹⁹) and IAA-producing bacteria (e.g., Bacillus spp., Pseudomonas spp., and Streptomyces spp.²²) were studied as high-level IAA-producing

cal/enzymatic reduction of IAA could result in tryptophol (6) possessing sleep-inducing activity in humans and serving as a reactant for Colletotryptin A synthesis (7).⁸ In addition, the compound could be converted to furoindolines and halofuroindolines, active pharmaceutical ingredients (APIs). Neoxaline (8), an antimitotic agent, can be synthesized *via* multistep cyclization starting from tryptophol.⁹⁻¹¹

^aSchool of Biomolecular Science and Engineering, Vidyasirimedhi Institute of Science and Technology (VISTEC), Wangchan Valley, Rayong, 21210, Thailand. E-mail: Nopphon.we@eng.buu.ac.th

^bFuture Biomanufacturing Research Hub (FBRH), Manchester Institute of Biotechnology, Department of Chemistry, The University of Manchester, Manchester M17DN UK

^cDepartment of Chemistry, National University of Singapore, 3 Science Drive 3, 117543, Republic of Singapore

^dDepartment of Chemical Engineering, Faculty of Engineering, Burapha University, Chonburi 20131. Thailand

 $[\]dagger$ Electronic supplementary information (ESI) available. See DOI: https://doi.org/10.1039/d4gc05236f

Paper

Fig. 1 Examples of bioactive compounds synthesized from indole-3acetic acid and its derivatives: indole-3-acetic acid (1), indole acetic acid sulfonate derivatives (2),⁵ Arcyriaflavin A (3),⁶ indole-3-acetaldehyde (4), deschloro 12-*epi*-fischerindole W nitrile (5),⁷ tryptophol Collectryptin A (7),8 and Neoxaline (8).7

microbes. Nevertheless, Escherichia coli is the most attractive host employed in the large-scale production of IAA due to the availability of genetic tools.23,24

Nevertheless, the whole-cell bioconversion yielded low productivity because IAA is a secondary metabolite, leading to lower protein expression in its IAA biosynthesis. Alternatively, the chemical synthetic route was proposed to convert glutamic acid, a low-cost precursor, to IAA via Fischer ring closure. However, the yield obtained from the multistep reaction was relatively low (~10.17%).25 Moreover, enzymatic reactions have been explored to replace conventional whole-cell bioconversion, particularly for pharmaceutical and fine chemical syntheses, where high specificity and selectivity are essential. 26,27

In addition to developing synthetic routes, process engineering is also crucial for scalable and efficient chemical transformations. Biocatalytic reactions implemented in a continuous flow reactor-often referred to as flow biocatalysisprovide several advantages, including improved gas-liquid transfer, streamlined process integration, and a simplified recycling scheme.²⁸ Biocatalysts are usually immobilized for an easy setup in a flow reactor, enabling cascade reactions to be easily arranged in sequence. In our recent study, we showcased a two-step biosynthesis of wax esters using metabolically engineered cells and in vitro enzyme catalysis in cascading flow reactors. 29

The modularity of flow reactor integration is beneficial, particularly for incompatible multistep syntheses where catalysts

in chemo-enzymatic reactions often cannot be used together. The catalyst deactivation can be avoided by separating reactions into different flow reactors. For example, (E)-4-hydroxystilbene was produced by the continuous-flow cascade of enzymatic phenolic acid decarboxylation and Pd-catalyzed Heck cross-coupling reactions.³⁰ Grossamide was produced by coupling amidation with a peroxidase-catalyzed reaction.³¹ Such telescoped flow synthesis prevented enzyme denaturation, which could occur due to reagents or harsh conditions used in the chemical reaction step.

In this work, IAA was synthesized via two-step reactions. First, L-tryptophan (L-Trp) was converted to indole-3-acetamide (IAM) via tryptophan 2-monooxygenase (TMO)-catalyzed oxidative decarboxylation. Then, IAM underwent acid-catalyzed hydrolysis into IAA at a relatively high temperature. As the enzyme could potentially be denatured upon acid addition and heating, the two-step processes were telescoped into cascading flow reactors. To effectively streamline the flow reactions, we developed a method for immobilizing TMO and designed flow reactor operations based on empirical kinetics. The key result from this work is the telescoped setup for gramscale synthesis of IAA, with high productivity and efficiency.

Results and discussion

Immobilization methods of the TMO enzyme

We examined five immobilization methods and compared them in terms of the percentage of enzyme loading efficiency, percentage of relative activity, and reusability (Table 1 and S1, ESI†). Chitosan was used as the solid support. The five methods were classified into two modes based on the types of interactions between TMO and supports: covalent-based and coordinationbased. For the covalent-based mode, three methods were tested using different functionalizing agents: 1,4-butanediol diglycidyl ether (Epx), glutaraldehyde (Glu), and glutaraldehyde-polyethylenimine-glutaraldehyde (Glu@PEI@Glu). For the coordinationbased mode, two methods were tested using glutaraldehyde-NTA-Ni²⁺ (Glu@NTA-Ni²⁺) and the commercially available chelating SepharoseTM Fast Flow.

For the covalent-based mode, the Epx and Glu samples showed very low relative activities and relatively low loadings. Among all the covalent-based methods, the Glu@PEI@Glu sample exhibited the highest loading efficiency. The maximum loading of 6.35 \pm 0.09 mg_{TMO} g_{support}⁻¹ was obtained within 6 h. A longer immobilization time did not significantly change the relative activity. However, we observed that Glu@PEI@Glu showed an unexpected increase in activities over the 2nd and $3^{\rm rd}$ cycles (28.99 ± 3.76% and 37.97 ± 5.06%, respectively). We later found that the phenomenon was from the adsorption of L-Trp and IAM (S2, ESI†).

For the coordination-based mode, the Glu@NTA-Ni²⁺ sample yielded promising results in terms of relative activity and reusability. Regardless of the immobilization time, the relative activities were similar (about 32.87 ± 3.26%), indicating that the immobilization time did not affect their function.

Green Chemistry Paper

Table 1 The screened immobilization methods for TMO at various immobilization times (2, 4, 6, and 8 h)

		Loading efficiency $(mg_{TMO} g_{support}^{-1})$			% relative activity				Loading Efficiency	
Method	Structure	2 h	4 h	6 h	8 h	2 h	4 h	6 h	8 h	Low
Glu		3.55 ± 0.13	3.94 ± 0.54	4.84 ± 0.10	5.68 ± 0.70	17.80 ± 7.01%	17.79 ± 5.54%	14.41 ± 5.99%	23.14 ± 15.06%	
Ерх	OTHER SHIP	1.27 ± 2.98	1.40 ± 3.97	1.35 ± 3.30	1.50 ± 2.16	22.05 ± 5.63%	15.88 ± 2.68%	$14.66 \pm 5.56\%$	$12.47 \pm 8.73\%$	
Glu@PEI@Glu	Outstand	4.31 ± 0.22	5.82 ± 0.02	6.35 ± 0.09	6.14 ± 0.12	16.64 ± 3.76%	17.94 ± 3.69%	19.04 ± 4.25%	$18.44 \pm 5.56\%$	High Relative Activity Low
Glu@NTA-Ni ²⁺		0.71 ± 0.54	0.93 ± 0.45	1.14 ± 0.40	1.58 ± 0.33	29.48 ± 5.65%	33.46 ± 0.09%	35.68 ± 0.22%	30.68 ± 1.02%	
Chelating Sepharose $^{\text{TM}}$ Fast Flow		5.30 ± 0.63	5.64 ± 0.37	5.40 ± 0.29	5.49 ± 0.44	71.72 ± 2.10%	68.10 ± 1.53%	72.12 ± 4.75%	64.82 ± 6.43%	High

The times indicated in the table refer to the immobilization time. Blue spheres represent chitosan beads, and the orange sphere represents Sepharose.

The reusability remained unchanged within three cycles. However, this Glu@NTA-Ni²⁺ method was limited by the low enzyme loading efficiency, with the maximum loading of 1.58 \pm 0.33 $mg_{TMO}\ g_{support}^{-1}$ for 8 h immobilization time. Therefore, we decided to perform immobilization with the commercially available SepharoseTM Fast Flow. At the optimal immobilization time of 2 h, a high loading of 5.30 \pm 0.63 $mg_{TMO}\ g_{support}^{-1}$ was obtained, approximately a 3.4-fold increase from the Glu@NTA-Ni²⁺ method. The percentage of relative activity in the first cycle was 69.19 \pm 4.20%, and the reusability remained constant for three cycles, indicating the high stability of the immobilized TMO.

According to these immobilization developments, we found that the covalent-based mode could result in a high loading efficiency due to their random interactions, increasing the chance of interactions with amino groups on the proteins. Nevertheless, such non-specific interactions could potentially cause conformational changes or blocking of active sites, thereby lowering the activity and stability of the enzyme (*i.e.*, less reusable). On the other hand, the coordination-based mode showed high activity and reusability. Altogether, we selected the chelating SepharoseTM Fast Flow for subsequent experiments.

Design equation of the flow enzymatic unit

As TMO was immobilized onto spherical resins, a packed bed reactor was selected for the flow enzymatic unit. To estimate the amount of the immobilized TMO required for a specific reaction extent (*i.e.*, conversion), we developed a design equation based on a general design equation for a packed bed reactor (eqn (1)).³²

$$w = F_{A0} \int_0^x \frac{\mathrm{d}x}{-r_{A}'} \tag{1}$$

where F_{A0} is the initial molar flow rate of the L-Trp substrate (nmol s⁻¹), x is the conversion, $-r'_{A}$ is the specific rate of the reaction (nmol s⁻¹ g_{cat}^{-1}), and w is the weight of the catalyst (g_{cat}).

The reaction rate of TMO-catalyzed decarboxylation can be expressed using Michaelis-Menten kinetics, as in eqn (2), assuming that external mass transfer is relatively fast.

$$-r_{\rm A}' = \frac{V_{\rm max}'S}{K_{\rm M} + S} \tag{2}$$

where S is the substrate concentration (μ M), $K_{\rm M}$ is the Michaelis–Menten constant (μ M), and $V'_{\rm max}$ is defined as the specific turnover number with the unit of nmol s⁻¹ g_{cat}⁻¹, representing the maximum velocity ($V_{\rm max}$) obtained per gram of catalyst.³³ Through $V'_{\rm max}$, the intraparticle diffusional resistance has been incorporated. $V'_{\rm max}$ was experimentally determined by plotting the initial velocities (nmol s⁻¹ g_{cat}⁻¹) against the concentrations of the substrate (μ M). The conversion can be written in terms of a substrate concentration, as in eqn (3) and (4):

$$x = \frac{S_0 - S}{S_0} = 1 - \frac{S}{S_0} \tag{3}$$

$$\mathrm{d}x = -\frac{1}{S_0}\mathrm{d}S\tag{4}$$

Combining eqn (2) and (4) with eqn (1), we can derive the following analytical expression (eqn (5)):

$$w = -\frac{F_{A0}}{V'_{\text{max}}S_0}K_M \ln(1-x) + \frac{F_{A0}}{V'_{\text{max}}S_0}xS_0$$
 (5)

The initial molar flow rate of the substrate can be expressed in terms of volumetric flow rate (Q, mL s⁻¹) and substrate concentration (μ M), as in eqn (6).

$$F_{A0} = Q \cdot S_0 \tag{6}$$

Therefore, eqn (5) can be transformed into eqn (7):

$$w = \frac{Q}{V'_{\text{max}}} (xS_0 - K_{\text{M}} \ln(1 - x))$$
 (7)

The steady-state kinetics was investigated to determine the kinetic parameters related to the reaction rate of immobilized TMO, as in Fig. 2A. The value of $K_{\rm M}$ of immobilized TMO was

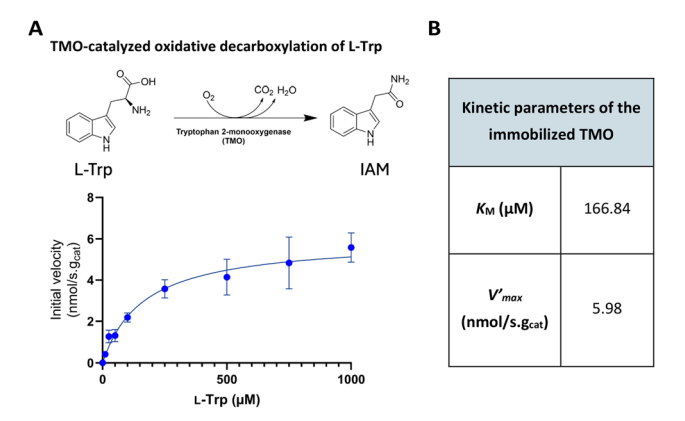


Fig. 2 The kinetic parameters of immobilized TMO on the SepharoseTM Fast Flow: (A) Michaelis–Menten plot between the initial velocity (nmol s⁻¹ g_{cat}^{-1}) and the concentration of L-Trp (μ M) and (B) the K_M and V'_{max} values of immobilized TMO.

166.84 μ M, and V'_{max} was 5.98 nmol s⁻¹ g_{cat}^{-1} as shown in Fig. 2B. The turnover number (k_{cat}) was calculated to be 1.58 s⁻¹, corresponding to the catalytic efficiency $(k_{cat}/K_{\rm M})$ of 9.47 mM⁻¹ s⁻¹. By comparing the values with the wild-type TMO reported in the previous study (92.8 μ M $K_{\rm M}$, 8.07 s⁻¹ $k_{\rm cat}$, 87.0 mM⁻¹ s⁻¹ $k_{\rm cat}/K_{\rm M}$), 34 the data confirm that the immobilization affected the enzyme activities in two ways. First, the immobilization reduced the ability of TMO to react with L-Trp (*i.e.*, higher $K_{\rm M}$). The access of the substrate to the active site or catalytic pocket of the enzyme could potentially be affected. Second, the catalytic turnover of the enzyme was reduced (*i.e.*, lower $k_{\rm cat}$), which could be caused by the conformational changes of the enzyme. The immobilization might restrict the enzyme dynamics, affecting the kinetic parameters.

Using the empirical kinetics along with the analytical design equation (eqn (7)), we can generate the predicted amount of immobilized TMO required at different operating conditions (Fig. 3). Flow rates (Q: 0.003–0.011 mL s⁻¹) and L-Trp concentrations (S_0 : 500–5000 μ M) were varied while setting the target conversions (x) as 0.70 and 0.80. The amount of immobilized TMO increased linearly with the L-Trp concentration and flow rate. The conversion becomes increasingly important at a higher L-Trp concentration and flow rate.

Validation of the design equation of the flow enzymatic unit

To validate the design equation, we performed the experiment on the flow enzymatic unit under target conditions (the conversion, x = 0.99). The basis operating conditions were set with Q as 9.25×10^{-3} mL s⁻¹ and S_0 as 4000 μ M. The predicted amount of catalyst (w) was 8.84 g. As the weight of the catalyst was mainly from the weight of the resin (i.e., 0.02% of g_{TMO} in g_{cat}), the density of the resin (1.01 g mL⁻¹) was used to estimate the volume of the catalyst. Assuming a void fraction of 0.4, the reactor volume was estimated to be 14.59 mL.

The experimental result of enzymatic unit validation is shown in Fig. 4. The averaged steady-state concentration of

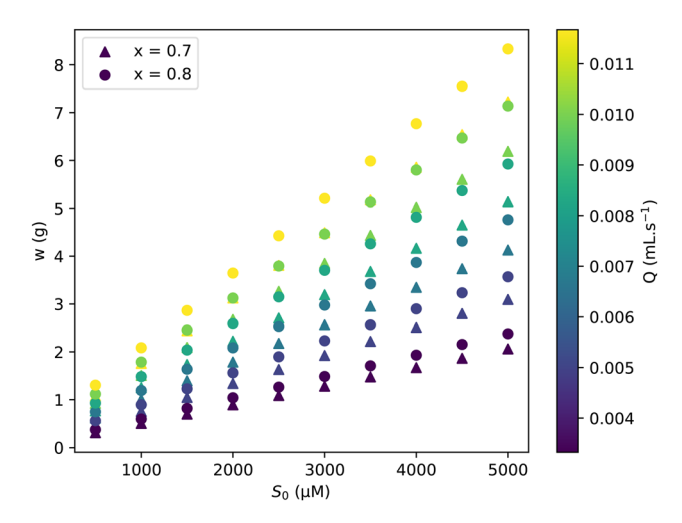


Fig. 3 The relationship between the volumetric flow rate (Q, mL s⁻¹), the initial concentration of the substrate (S_0 , μ M), conversion (x), and the weight of the catalyst (w, g).

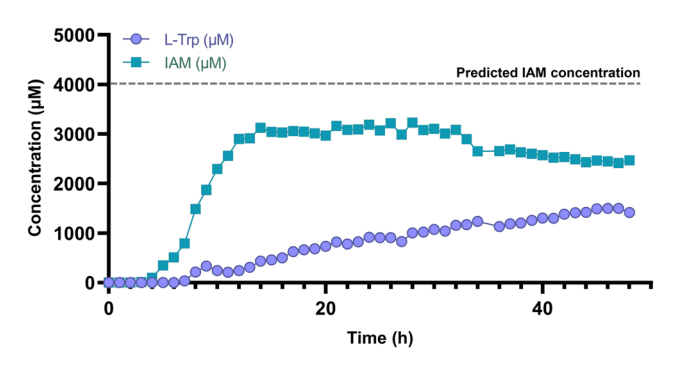


Fig. 4 The production of immobilized TMO under a continuous flow system for two days. (The dashed line represents the predicted value from the design equation.)

IAM was $3086 \pm 72 \, \mu\text{M}$, equivalent to the conversion (x) of 0.77. The production remained at a steady state for 18 h, from 14 h to 32 h, and a gradual decrease in IAM production was noticed after 32 h of operation. Note that the immobilized enzyme remained stable for 32 hours before its activity declined due to enzyme degradation. During the production, we also observed an increase in the remaining L-Trp over time during both the steady-state period and the later stage of production.

The gradual increase of L-Trp over time was likely due to the degradation of the enzyme and the accumulation of L-Trp. The latter was a result of the coordination between the functional group of L-Trp and divalent metal ions (Ni²⁺).³⁵ It is also important to note that the experimental conversion (0.77) was slightly lower than the target value (0.99), possibly due to multiple effects including the previously mentioned enzyme degradation and the wide residence time distribution in the packed bed reactor (*i.e.*, channeling through the voids of the packing).

Acid-catalyzed hydrolysis of IAM

Following the first enzymatic reaction, hydrolysis was used to convert IAM into IAA. Types of catalysts and concentrations were studied (S3, ESI†). An acid (HCl) could catalyze the hydrolysis of amide species to carboxyl species faster than a base (NaOH). This could be explained by the mechanisms of the reactions. The product from the elimination step of acid-catalyzed hydrolysis (NH₃, weak base) is more stable than that of base-catalyzed hydrolysis (NH₂⁻, stronger base), indicating that the acid can generate a better leaving group as compared to the base (S4, ESI†), resulting in a faster reaction rate. The optimal conditions obtained from the experiments were 1 M HCl and 1 mM IAM.

The temperature could also affect hydrolysis. In this study, we explored the reaction temperature from 60 °C to 120 °C. Fig. 5 illustrates the percentage of IAM conversion and percent yield of IAA from the acid-catalyzed hydrolysis at varying temperatures. The IAA yield was found to be lower than the IAM conversion, suggesting that IAA may be degraded or converted to other side products upon these acidic and thermal conditions (IAA degradation at varying temperatures, S5, ESI†).

At a higher temperature, the conversion of IAM and the degradation of IAA, at the same time, were faster than those at lower temperatures resulting in a low yield of IAA. The IAA yields obtained were 31.11 \pm 2.60% and 21.99 \pm 0.15% when

Acid-catalyzed hydrolysis of IAM

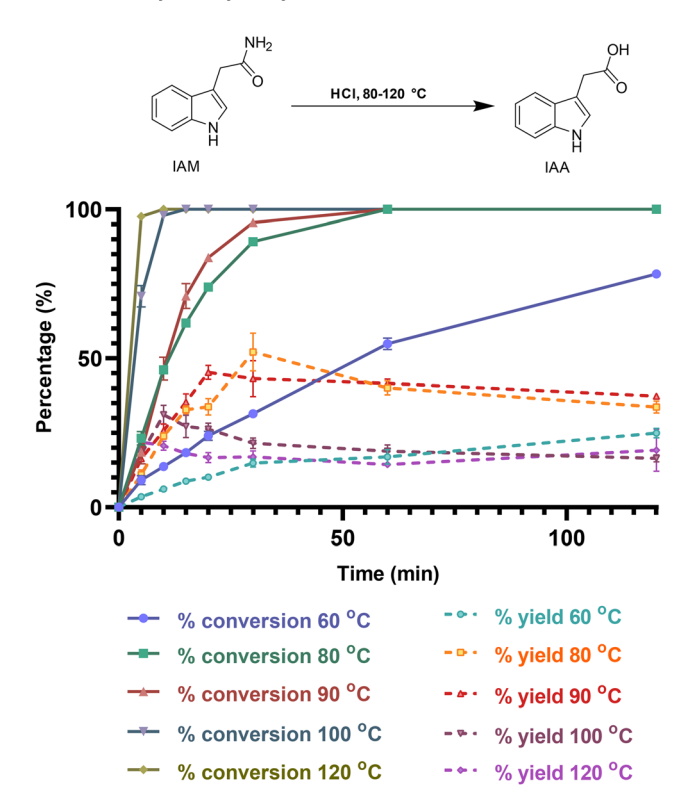


Fig. 5 The percentage of conversions and yields of IAM hydrolysis at various temperatures under batch conditions.

performed at 100 °C and 120 °C, respectively. On the other hand, at a relatively low temperature of 60 °C, a low yield of IAA was obtained (24.96 \pm 1.31%), due to the low conversion of IAM. Among all the temperatures tested, the temperature of 80 °C was selected as it offered the highest IAA yield of 52.10 \pm 5.19%.

Design equation of the flow hydrolysis unit

Similar to the flow enzymatic unit, we developed the design equation for the flow hydrolysis unit. Since the reaction was in a homogeneous liquid phase, the hydrolysis would be conducted in a tubular reactor. In order to determine optimal operating conditions, we need to identify the optimal residence time where IAM conversion was maximized and IAA degradation was minimized. The kinetics of IAM conversion was assumed to be of pseudo-first order, as in eqn (8).

$$-r_{A} = \frac{dC_{IAM}}{dt} = k_{1}C_{IAM}$$
 (8)

eqn (8) can be integrated over a residence time of the flow reactor to obtain eqn (9).

$$C_{\text{IAM}} = C_{\text{IAM0}} e^{-k_1 \tau} \tag{9}$$

The change in IAA concentration could be due to IAA formation (due to IAM conversion) and thermal IAA degradation. If the degradation was assumed to be first-order, the kinetics of IAA could be written as in eqn (10).

$$\frac{\mathrm{d}C_{\mathrm{IAA}}}{\mathrm{d}t} = k_1 C_{\mathrm{IAM}} - k_2 C_{\mathrm{IAA}} \tag{10}$$

We can substitute eqn (10) with eqn (9) to obtain eqn (11).

$$\frac{dC_{IAA}}{dt} = k_1 C_{IAM0} e^{-k_1 \tau} - k_2 C_{IAA}$$
 (11)

Solving eqn (11), which is the ordinary differential equation, we can obtain an analytical expression of the IAA concentration (eqn (12)):

$$C_{\text{IAA}} = \frac{k_1 C_{\text{IAM0}}}{k_2 - k_1} \left[e^{-k_1 \tau} - e^{-k_2 \tau} \right]$$
 (12)

To determine optimal conditions (*i.e.*, maximum IAA concentration), the derivative of the IAA concentration was set to zero eqn (13).

$$\frac{\mathrm{d}C_{\mathrm{IAA}}}{\mathrm{d}\tau} = 0\tag{13}$$

Solving eqn (13), we identified the optimal residence time to be written in terms of the kinetic parameters of the IAM conversion and IAA degradation, as in eqn (14).

$$\tau_{\text{opt}} = \frac{\ln \frac{k_2}{k_1}}{(k_2 - k_1)} \tag{14}$$

The rate constants of the reactions were experimentally determined at 80 °C (Table 2). The optimal residence time

Paper

 Table 2
 The rate constants of IAM conversion and IAA degradation by

Table 2 The face constants of with conversion and with acquadion	D y
acid-catalyzed hydrolysis at 80 °C	

Reaction	Rate constant (s ⁻¹)
IAM conversion (k_1)	9.18×10^{-4}
IAA degradation (k_2)	2.42×10^{-4}

The rate constants were determined under the assumption that both IAM conversion and IAA degradation followed pseudo-first order kinetics (S6, ESI†).

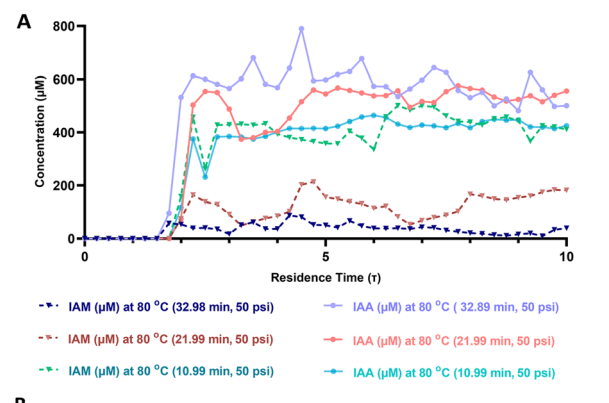
 $(\tau_{\rm opt})$ was predicted to be 32.98 min; therefore, the length of PFR (1.588 mm I.D.) was 9.22 m.

Validation of the design equation of the flow hydrolysis unit

The validation was performed under a continuous-flow system at 80 °C using a flow rate of 0.555 mL min $^{-1}$. We tested the hydrolysis unit at three different residence times: 32.98 min (the predicted value of $\tau_{\rm opt}$), 21.99 min (2/3 of $\tau_{\rm opt}$), and 10.99 min (1/3 of $\tau_{\rm opt}$). Using 10.99 min of residence time, the reaction was incomplete with 58.14% conversion and 41.41% IAA yield. On the other hand, as in Fig. 6, there were no noticeable differences in the percentage of yield and percentage of selectivity – between 32.98 min and 21.99 min, suggesting that even shortening the residence time from the predicted value could still maintain a similar reaction extent. Therefore, a residence time of 21.99 min was selected for the flow hydrolysis unit.

Telescoped chemo-enzymatic synthesis of IAA

The flow enzymatic unit and flow hydrolysis unit were combined to construct a telescoped system for IAA synthesis as shown in Fig. 8. The products from the first and second reactive steps were confirmed using mass spectrometry analysis



 Residence time
 % conversion
 % yield
 % selectivity

 32.98 min
 96.06 ± 1.81 %
 58.51 ± 6.10 %
 60.91 ± 6.45 %

 21.99 min
 85.90 ± 3.95 %
 53.58 ± 2.60 %
 62.37 ± 3.95 %

 10.99 min
 58.14 ± 5.12 %
 41.41 ± 4.06 %
 71.22 ± 9.39 %

Fig. 6 (A) The validated results including yields of IAA and residual IAM under a flow system with an IAM feeding concentration of 2 mM, 80 °C, 50 psi. Three sets of residence times include 32.98, 21.99, and 10.99 min. (B) The percentage of conversion, yield, and selectivity from each residence time.

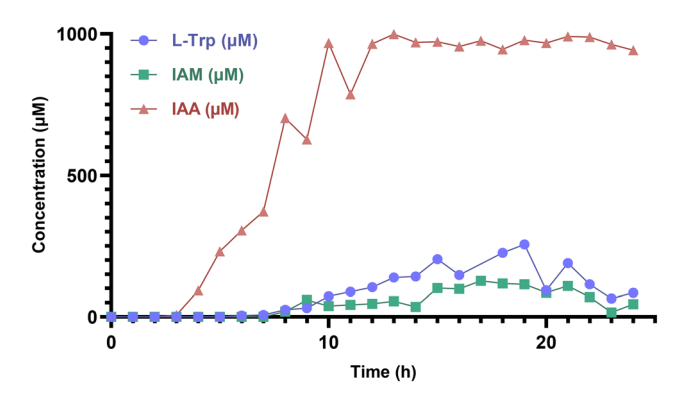


Fig. 7 The telescoped chemo-enzymatic synthesis of IAA within 24 hours.

(see S7 and S8 in the ESI†). The telescoped setup was performed for 24 h (Fig. 7). The IAA yield reached a steady state at the 12th hour with an overall yield of 970.10 \pm 16.23 μ M (0.1699 \pm 0.0028 mg mL⁻¹). The space-time yield (STY) of the process was calculated based on eqn (15):³⁶

Space-time yield (STY) =
$$\frac{m_{\rm p}}{\tau V_{\rm R}}$$
 (15)

where m_p is the amount of product (g) formed within the residence time (day) and V_R is the applied reaction volume (L).

The experimental yield percentage was calculated based on eqn (16).

$$\% \text{ yield} = \frac{C_{\text{product}} Q_{\text{out}}}{C_{\text{substrate}} Q_{\text{in}}}$$
 (16)

where C_{product} is the concentration of the product or IAA (mM), Q_{out} is the outlet flow rate (mL min⁻¹), $C_{\text{substrate}}$ is the concentration of the substrate (mM), and Q_{in} is the inlet flow rate (mL min⁻¹).

In this work, the productivity of the process was 11.16 g L^{-1} day⁻¹ with an overall yield of 48.50%. STY represents productivity while the yield represents a resource or substrate utilization efficiency. The experimental yields were found to be higher than the expected yields (41.26% - 77% and 53.58% from the enzymatic and hydrolysis units, respectively). This slight improvement could be influenced by the residual buffer from the enzymatic unit which may have mitigated the harshness of the conditions during the hydrolysis step (S9, ESI†). Additionally, the residual L-Trp could also be consumed - the concentration of the residual L-Trp was lower than the theoretical calculation, indicating that L-Trp was converted to other species in the hydrolysis reactor - decreasing the concentration of acid in the system. Moreover, we also performed the isolation of the final product (IAA). Through chromatography and ¹H NMR analysis (see S10 in the ESI†), we found that an isolated yield of 42.21% was obtained.

Table 3 compares the STY and yield of this work with those in previous reports. Most whole-cell bioconversions or fermentations gave high yields, but relatively low productivity. On the other hand, the chemical-based transformation resulted in

Fig. 8 Schematic continuous-flow chemo-enzymatic synthesis of IAA developed in this work

Table 3 The comparison of different methods for the production of IAA

Method	Substrate	STYa (g L-1 day-1)	% Yield ^b	Ref.
Fermentation	ь-Trp	0.89	79.25%	38
Fermentation	ь-Trp	3.55	82.78%	24
Fermentation	ь-Trp	0.79	58.94%	39
Enzymatic cascade	Indole	0.86	57.50%	40
Chemical synthesis ^c	Indole	18.96	35.20%	37 and 41
Chemical synthesis	Glutamate	72.73	10.17%	25
Chemo-enzymatic flow synthesis	L-Trp	11.16	48.50% ^d	This work

 a STYs were calculated based on the final step of the process (In this study, the calculation was based on the hydrolysis unit). b % yield was calculated based on the amount of product produced relative to the initial amount of the main substrate added to the working processes. c The reaction required sodium cyanide, a deadly toxic compound, using which practical safety was a concern. d The isolated yield of our system was 42.21%.

higher values of STY, commonly ranging from 10 to 100 g $\rm L^{-1}$ day⁻¹; however, the yields achieved from the routes were lower than those of bioconversions. The low yields were the result of low selectivity and product loss during work-up steps and multi-step syntheses. In this work, we leveraged the advantages of biocatalysis and chemical reactions, compromising the productivity and yield. Unlike the fermentation, the continuous-flow setup in this study can be easily scaled. This chemo-enzymatic setup also eliminates the use of toxic reagents typically found in chemical synthesis routes (*e.g.* phenylhydrazine, ²⁵ sodium cyanide. ³⁷)

Experimental section

Materials and analytical instruments

L-Tryptophan (>98.5%), indole-3-acetamide (>98.0%), indole-3-acetic acid (>98.0%), and other standard chemicals were purchased from Tokyo Chemical Industry (TCI) Co. Ltd. $N\alpha$, $N\alpha$ -Bis(carboxymethyl)-L-lysine hydrate (>97.0%), 25% glutaraldehyde in water (grade II), PEI (MW = 10000, branched),

37% fuming hydrochloric acid, 100% acetic acid (glacial), and other organic solvents were purchased from Sigma-Aldrich™. Chitosan (90.0% deacetylated degree) was purchased from Glentham LIFE SCIENCES. 1,4-Butanediol diglycidyl ether (93%) was purchased from FUJIFILM Wako Chemical Co. Ltd. The reagents for molecular construction were purchased from New England BioLabs Inc. Chelating Sepharose™ Fast Flow was purchased from Cytiva Inc. The HPLC column and the HPLC instrument were from Agilent Technologies Inc.

TMO plasmid construction, expression and purification

The codon-optimized TMO gene (*iaaM*) fragment was inserted into the pET15b plasmid at the *BamH*I and *Nde*I restriction sites to obtain the pET15b-*iaaM* plasmid. The sequence was verified by DNA sequencing.

The methods of TMO expression and purification were modified from Kongjaroon et al.34 The pET15b-iaaM plasmid and pGro7 chaperone were transformed into E. coli BL21 (DE3) using the heat shock method. The cells were grown on agar plates containing 50 $\mu g \text{ mL}^{-1}$ of ampicillin and 20 $\mu g \text{ mL}^{-1}$ chloramphenicol to select the transformants. Protein expression was induced by the auto-induction method. The 10 mL starter was prepared by single colony inoculation into a ZY medium containing 50 μg mL⁻¹ ampicillin and 20 μg mL⁻¹ chloramphenicol. The starter culture was incubated overnight at 37 °C, 220 rpm, and subsequently inoculated with 1% inoculation into 650 mL of ZY-rich medium containing the same antibiotics with 0.5 mg mL⁻¹ L-arabinose for GroEL-ES chaperone induction. The incubation conditions were controlled at 37 °C, 220 rpm until OD₆₀₀ reached the range of 0.8-1.0. The temperature, subsequently, was adjusted to 25 °C, and the incubation was continued for 16-18 h. The cells were harvested by centrifugation at 4 °C, 10 876g for 15 minutes to obtain cell pellets.

For TMO purification, the cell pellet was resuspended by 200 mL of 50 mM Tris-HCl buffer, pH 8.3, containing 10 mM imidazole, 0.1 mM phenylmethylsulfonyl fluoride (PMSF), and 200 mM NaCl. Ultrasonication was used to lyse the cells, and the lysate was centrifuged at 4 $^{\circ}$ C, 18 514g for 30 min to

remove the cell debris. Polyethylenimine (PEI) was added into The glutaraldehyde-functionalized beads were then washed with DI water three times. The NTA solution was prepared by adding Nα, Nα-bis(carboxymethyl)-L-lysine hydrate (NTA) into 0.1 M HEPES buffer, pH 8.0 to obtain the solution with a concentration of 0.05% w/v. The beads were added to the NTA solution and orbitally shaken overnight at 37 °C. The resulting beads (NTA-glutaraldehyde-functionalized chitosan beads) were washed with DI water three times before incubating with 0.2 M Ni²⁺ solution overnight at room temperature. The "Glu@NTA-Ni⁺²" bead samples were obtained. The beads were then washed with DI water three times and the reaction buffer (50 mM Tris-HCl buffer, pH 8.3) three times before storage in the reaction buffer for further study. Immobilization procedures. The enzyme solution was added

the supernatant, with a final concentration of 0.1%, to precipitate the DNA and remove it by centrifugation. The supernatant was loaded onto a nickel-chelating column (Ni-column); the column was pre-equilibrated with 50 mM Tris-HCl buffer, pH 8.3, holding 10 mM imidazole and 200 mM NaCl. The column was washed with washing buffer (50 mM Tris-HCl, pH 8.3, containing 20 mM imidazole and 200 mM NaCl) before the linear gradient of imidazole ranging from 25 to 250 mM was set to elute the proteins. The collected protein fractions were spectrophotometrically analyzed at A280 and A466 to measure total protein and TMO-bound FAD, respectively; the extinction coefficient of TMO-bound FAD (A₄₆₆) was 11.4 mM⁻¹ cm⁻¹ (ref. 42) and that of TMO (A₂₈₀) was 91 385 M⁻¹ cm⁻¹. Pure fractions, judged by the SDS-PAGE technique, were pooled and concentrated using a 10 kDa molecular weight cut-off Amicon stirred cell (MERCK). The buffer system was exchanged by loading the concentrated protein solution onto a Sephadex G-25 column (GE Healthcare), pre-equilibrated with 50 mM Tris-HCl, pH 8.3, and 10% glycerol. The purified TMO was kept at −80 °C.

into the Tris-HCl buffer, pH 8.3, containing 20 mM imidazole and 100 mg of the immobilizing beads with a final enzyme concentration of 15 µM. For the chelating Sepharose™ Fast Flow (Ni-resin), 100 mg of Ni-incubated resin was prepared before TMO solution was added to achieve the concentration of 15 µM. Immobilization was performed on a benchtop shaker at 4 °C, 200 rpm. Immobilization times were varied from 2, 4, 6, and 8 h to examine the effect of immobilization time on the physical and chemical properties of the immobilized TMO. The enzyme solution was sampled to measure the residual enzyme in the solution after immobilization and compared to the initial amount of enzyme to calculate the loading efficiency (egn (17)):

TMO immobilization

% loading efficiency = $\frac{m_{\rm TMO,i} - m_{\rm TMO,f}}{m_{\rm b}}$ (17)

Chitosan bead preparation. Chitosan powder was dissolved in 1 M acetic acid to obtain 2% w/v chitosan solution. The resulting sample was ultrasonicated for 15 minutes to facilitate the dissolution. The coagulation solution was prepared by the addition of sodium hydroxide (NaOH) in 26% ethanol in water to obtain 1 M NaOH solution. The well-dissolved chitosan solution was then dripped into the coagulation solution using a syringe before magnetically stirring the beads for 40 minutes at room temperature. The beads were finally filtered out using a sieve (0.6 mm I.D. of pores), washed with 50 mM Tris-HCl buffer, pH 8.3, and kept in deionized (DI) water for the functionalization step.

where $m_{\rm TMO,i}$ is the initial amount of TMO before loading, $m_{\text{TMO,f}}$ is the final amount of TMO after loading, and m_{b} is the mass of immobilizing beads.

Functionalization of chitosan beads. For the covalent-based mode, there were three immobilization methods (Glu, Epx, Glu@PEI@Glu). For the "Glu" method, chitosan beads were added into 3% v/v glutaraldehyde solution (10 g beads per 100 mL solution.) The functionalization was performed by orbitally shaking at 200 rpm and 37 °C for 3 h. The beads were then washed with DI water three times; as a result, glutaraldehyde-functionalized chitosan (Glu) beads were obtained. For the "Epx" method, 1.25% v/v 1,4-butanediol diglycidyl ether was used to prepare epoxide-functionalized chitosan. For the "Glu@PEI@Glu" method, the glutaraldehyde-functionalized chitosan beads were modified to increase their branching by functionalizing the beads with polyethylenimine (PEI) solution at a ratio of 1:1. The obtained beads were then functionalized again with 1.25% glutaraldehyde solution, resulting in "Glu@PEI@Glu" beads.

In addition to the loading efficiency, we also measured the relative activity and reusability of the immobilized TMO. The substrate solution (L-Trp) was added to the buffer containing the immobilized TMO to initiate the enzymatic reaction. The substrate-to-TMO ratio of 1000 μM : 1.5 μM was controlled. The reaction was carried out for 10 min by shaking the mixture at 200 rpm and room temperature. The solution was sampled for HPLC analysis. The free enzyme experiment was set with the same amount of enzymes as that of the immobilized TMO. 1 M HCl with an equal volume to the sample was used to quench the reaction of the free enzyme reaction. The relative activity can be estimated using eqn (18):

For the coordination-based mode, we modified and optimized the method based on de Andrade et al. 43 Chitosan beads were added to 1.25% v/v glutaraldehyde solution (ratio of 10 g beads per 100 mL solution.) The functionalization was performed by orbital shaking at 200 rpm and 37 °C for 3 h.

$$\% \ relative \ activity = \left(\frac{Activity_{imTMO}}{Activity_{freeTMO}}\right) \times 100 \ \ (18)$$

where Activity_{imTMO} is the activity of the immobilized TMO and Activity_{freeTMO} is the activity of the free TMO.

Steady-state kinetics of immobilized TMO

In our study, we found that when TMO was immobilized on SepharoseTM Fast Flow resins, a loading of 2.35×10^{-4} g_{TMO} g_{resin}⁻¹ was obtained. The concentration of immobilized TMO stock solution was adjusted to 5 μ mol_{TMO} L_{total volume}⁻¹.

Green Chemistry Paper

A steady-state kinetic experiment was carried out following the protocol used in the previous study. The reactions were set in 4 mL of varying L-Trp substrate concentrations. L-Trp was added to initiate the reaction. The samples were taken from the reaction mixture within 1 min and quenched with 1 M HCl. The samples were filtered with a 0.22 μ m nylon filter prior to injection into a high-performance liquid chromatograph with a diode array detector system.

Acid-catalyzed hydrolysis of IAM

Stock solutions of IAM and HCl were separately prepared and placed in a sealed tube under constant magnetic stirring at 180 rpm. The final concentrations of IAM and HCl were 1 mM and 1 M, respectively. The effect of temperature on the reaction was examined. Five sets of experiments were conducted at different temperatures, including 60, 80, 90, 100, and 120 °C. Each set of experiments included nine reaction sealed tubes, assigned for a specific reaction time (0, 5, 10, 15, 20, 30, 60, 120, and 180 min). The reaction was conducted in three replicates. To quench the reaction, the samples were immediately placed on ice. Each sample was then diluted with an equal volume of dissolving solution. The quenched and diluted samples were immediately stored at −80 °C until they were ready for HPLC analysis. To simplify the experimental determination of kinetic parameters, the reaction was treated as a pseudo-first order (owing to the fact that the acid concentration was 1000-fold higher than the IAM concentration). The rate constant of hydrolysis (k_1) was calculated based on the half-life $(t_{1/2})$ of IAM during the IAM conversion (eqn (19)).

$$t_{1/2} = \frac{\ln 2}{k_1} \tag{19}$$

IAA degradation observation and its kinetics

HCl and IAA stock solutions were added to tightly sealed vials to achieve a final concentration of 1 mM IAA and 1 M HCl. The reactions were conducted at different temperatures to observe the degradation of IAA at various temperatures including 60, 80, 90, 100, and 120 °C. The reactions were magnetically stirred at 200 rpm throughout the reaction time (30 min).

The kinetics of IAA degradation was determined by treating the reaction as pseudo-first order. IAA stock solution was mixed with HCl to achieve the final concentration of 1 mM IAA and 1 M HCl. The optimized conditions achieved from acid-catalyzed hydrolysis were mimicked (80 °C reaction temperature). The reaction mixtures were separated into nine vials according to the different assigned reaction times (0, 5, 10, 15, 20, 30, 45, 60, and 120 min); each set was done with three replicates. All reactions were performed under magnetic stirring at 200 rpm and 80 °C. All quenched reaction samples were collected and stored under -80 °C until they were ready for HPLC analysis. For kinetic determination of IAM hydrolysis, the HPLC-analyzed data of IAA degradation were collected to do curve fitting and calculate the rate constant of IAA degradation (k_2) using the previous method (eqn (19)).

Setup of the continuous flow synthesis of IAA

For the enzymatic unit, L-Trp solution was flowed into the reactor using a syringe pump and mixed with an air flow using Tee assembly (IDEX); the volumetric flow rate was controlled at 0.2775 mL min⁻¹. The packed-bed reactor was sized based on the mass of the desired catalyst (TMO + resin) calculated from the design equation (eqn (7)). The result from the calculation was 8.76 mL of the immobilized TMO (including the mass of resins) and 14.59 mL of the reactor volume. A PFA tube (O.D. 12 mm × I.D. 10 mm, 185.8 mm long) was selected to construct a packed-bed reactor. Both ends of the column were connected to stainless steel 316-reducing unions, O.D. 1/2" × 1/8" (Hy-Lok, CUR-8-2-S316), with 30 μm-stainless 304 wire mesh filters to prevent the resins from eluting out from the reactor. The flow enzymatic unit was pre-equilibrated by flowing 50 mM Tris-HCl buffer, pH 8.3, for 10 column volumes. The flow reaction was performed under the target conditions ($Q = 9.25 \times$ $10^{-3} \text{ mL s}^{-1}$, $S_0 = 4 \text{ mM}$, x = 0.99), and the samples were collected every hour for 2 days.

For the hydrolysis unit, there were two feeding liquid solutions, IAM and HCl, which were mixed at the Tee assembly (IDEX). The tubular reactor for the hydrolysis comprised three main parts: the mixing region (MR), the heating region (HR), and the reaction region (RR). A PTFE tubing (3.175 mm O.D. \times 1.588 mm I.D.) was used for constructing the reactor. The length of the mixing region was based on the equation reported in Hartman *et al.*, 44 and the length of the heating region was based on Graetz's approximation.

Isolation of the final product IAA

The isolation was carried out by silica-based column chromatography using n-hexane: ethyl acetate (40:20) as a mobile phase. The purification was followed by thin-layer chromatography (TLC) under normal-phase conditions with a mobile phase including n-hexane, ethyl acetate, isopropanol, and acetic acid (40:20:5:1, v/v/v/v). The purified fractions were collected. The fractions were extracted with ethyl acetate and dried using anhydrous sodium sulfate. The solvent was subsequently removed using a rotary evaporator to prepare the sample for 1 H-NMR analysis. 1 H NMR $(400 \text{ MHz}, \text{DMSO-} d_6) \delta$: 12.17 (s, 1H, COOH), 10.90 (s, 1H, NH), 7.50 (d, J = 7.6 Hz, 1H), 7.35 (d, J = 8.0 Hz, 1H), 7.23 (s, 1H), 7.08 (t, J = 6.4 Hz, 1H), 6.98 (t, J = 6.8 Hz, 1H), 3.63 (s, 2H).

Chemical analysis

The reaction samples, after quenching, were centrifuged at 13 684.32g, 4 °C for 30 minutes before filtration using syringe 0.22 μ m nylon filters. A ZORBAX Eclipse Plus C18 (2.1 × 50 mm, 1.8 micron) column and a high-performance liquid chromatograph (Agilent Technologies 1260 Infinity II) equipped with a diode array detector (DAD) were used for the analysis. The mobile phase used was water with 0.5% formic acid (solvent A) and acetonitrile (solvent B). The conditions were set to increase the percentage of solvent B from 5% to 50% within 5 min and maintain the solvent ratio for 1 min

before increasing it to 100% and maintaining it for 1 min. The flow rate of the mobile phase remained constant at 0.2 mL min $^{-1}$ throughout the analysis; the temperature of the sampler and column was 25 °C. UV absorbance was monitored at 280 nm. HPLC analysis was validated using an external standard. Standard compound solutions were freshly prepared at concentrations ranging from 5 to 1000 μM to generate a standard curve for each analysis round. A high linearity was achieved (see S11 in the ESI†). The HPLC-DAD was also equipped with a mass spectrometer (Agilent Technologies InfinityLab LC/MSD). The MS analysis was used to confirm the identities of the compounds in the product sample.

Conclusions

In summary, we developed a method for synthesizing IAA by exploiting the advantages of an enzymatic reaction, chemical hydrolysis, and a continuous-flow system. The design equation of the flow enzymatic unit was developed to predict the required amount of enzymes while the kinetics of the IAA formation was formulated. The two reactive steps were telescoped. The space-time yield of the whole process was 11.16 g $\rm L^{-1}$ day⁻¹ with an overall yield of 48.50% across two steps and an isolated yield of 42.21%, highlighting the efforts to boost productivity while maintaining the production efficiency of the process.

List of notation

See the ESI.†

Author contributions

S. M.: conceptualization, investigation, methodology, data curation, formal analysis, visualization, and writing - original draft. S. K.: methodology, formal analysis, and review & editing. D. T.: supervision and reviewing & editing. C. K.: methodology and formal analysis. J. W. formal analysis and reviewing & editing. P. C.: formal analysis, resources, supervision, and reviewing & editing. N. W.: conceptualization, formal analysis, resources, supervision, project administration, writing – original draft, and funding acquisition.

Data availability

The authors certify that all main and supporting data have been reported in the main manuscript and in the ESI.†

Conflicts of interest

There are no conflicts to declare.

Acknowledgements

S. M. would like to acknowledge the scholarship from VISTEC. This work was financially supported by AUN/SEED-Net and JICA (grant number: BUU REd-UC 2401), the Faculty of Engineering at Burapha University (grant number: Opc.2/2567), and the NSRF via PMU-B Research and Innovation (grant number: B05F640089). We would like to acknowledge additional support from Burapha University and VISTEC.

References

- 1 A. W. Woodward and B. Bartel, *Ann. Bot.*, 2005, **95**, 707-735
- 2 S. Fu, J. Wei, H. Chen, Y. Liu, H. Lu and J. Chou, *Plant Signaling Behav.*, 2015, **10**, e1048052.
- 3 S. Paque and D. Weijers, BMC Biol., 2016, 14, 1-5.
- 4 D. Chen, Y. Chen, Z. Ma, L. Zou, J. Li and Y. Liu, *J. Org. Chem.*, 2018, **83**, 6805–6814.
- 5 M. S. K. Jadoon, J. Pelletier, J. Sévigny and J. Iqbal, RSC Adv., 2023, 13, 29496–29511.
- 6 J. Bergman, E. Koch and B. Pelcman, J. Chem. Soc., Perkin Trans. 1, 2000, 2609–2614.
- 7 A. Palmieri and M. Petrini, Nat. Prod. Rep., 2019, 36, 490-530.
- 8 W. Saetae, C. Chantana, S. Saithong, K. Chayajarus and J. Jaratjaroonphong, *J. Org. Chem.*, 2024, **89**(12), 8620–8631.
- 9 T. Hirose, T. Sunazuka, D. Yamamoto, N. Kojima, T. Shirahata, Y. Harigaya, I. Kuwajima and S. Ōmura, Tetrahedron, 2005, 61, 6015–6039.
- 10 T. Ideguchi, T. Yamada, T. Shirahata, T. Hirose, A. Sugawara, Y. Kobayashi, S. Ōmura and T. Sunazuka, J. Am. Chem. Soc., 2013, 135, 12568–12571.
- 11 T. Sunazuka, T. Shirahata, S. Tsuchiya, T. Hirose, R. Mori, Y. Harigaya, I. Kuwajima and S. Ōmura, *Org. Lett.*, 2005, 7, 941–943.
- 12 V. Report, Global Indole-3-acetic Acid (IAA) Market Insights, Forecast to 2030, https://reports.valuates.com/market-reports/QYRE-Auto-37N515/global-indole-3-acetic-acid-iaa, (accessed August 20, 2024, 2024).
- 13 C. Research, Indole 3 acetic Acid Market Size, Capacity, Demand & Supply 2023, https://www.24chemicalresearch. com/reports/200647/global-indoleacetic-acid-market-2023-2029-205, (accessed August 20, 2024, 2024).
- 14 H. Kasahara, Biosci., Biotechnol., Biochem., 2016, 80, 34-42.
- 15 D.-W. Di, C. Zhang, P. Luo, C.-W. An and G.-Q. Guo, *Plant Growth Regul.*, 2016, **78**, 275–285.
- 16 Y. Mano and K. Nemoto, J. Exp. Bot., 2012, 63, 2853-2872.
- 17 H. Etesami and B. R. Glick, Microbiol. Res., 2024, 127602.
- 18 J. Tang, Y. Li, L. Zhang, J. Mu, Y. Jiang, H. Fu, Y. Zhang, H. Cui, X. Yu and Z. Ye, *Microorganisms*, 2023, 11, 2077.
- 19 S. Soponputtaporn, M. Srithaworn, Y. Promnuan, P. Srirat and O. Chunhachart, *Trends Sci.*, 2024, 21, 7335–7335.
- 20 L. G. Sarmiento-López, M. López-Meyer, I. E. Maldonado-Mendoza, F. R. Quiroz-Figueroa, G. Sepúlveda-Jiménez and M. Rodríguez-Monroy, J. Biosci. Bioeng., 2022, 134, 21–28.

- 21 S. Emami, H. A. Alikhani, A. A. Pourbabaei, H. Etesami, F. Sarmadian and B. Motessharezadeh, *Int. J. Environ. Res.*, 2019, **13**, 603–611.
- 22 S. Manulis, H. Shafrir, E. Epstein, A. Lichter and I. Barash, *Microbiology*, 1994, **140**, 1045–1050.
- 23 D. Guo, S. Kong, X. Chu, X. Li and H. Pan, J. Agric. Food Chem., 2019, 67, 8186–8190.
- 24 H. Wu, J. Yang, P. Shen, Q. Li, W. Wu, X. Jiang, L. Qin, J. Huang, X. Cao and F. Qi, J. Agric. Food Chem., 2021, 69, 1916–1924.
- 25 S. W. Fox and M. W. Bullock, J. Am. Chem. Soc., 1951, 73, 2754–2755.
- 26 C. T. Walsh and B. S. Moore, *Angew. Chem., Int. Ed.*, 2019, **58**, 6846–6879.
- 27 E. Ricca, B. Brucher and J. H. Schrittwieser, *Adv. Synth. Catal.*, 2011, 353, 2239–2262.
- 28 A. Naramittanakul, S. Buttranon, A. Petchsuk, P. Chaiyen and N. Weeranoppanant, *React. Chem. Eng.*, 2021, **6**, 1771–1790.
- 29 S. Buttranon, J. Jaroensuk, P. Chaiyen and N. Weeranoppanant, Org. Process Res. Dev., 2024, 28, 1990–1997.
- 30 B. Grabner, A. K. Schweiger, K. Gavric, R. Kourist and H. Gruber-Woelfler, *React. Chem. Eng.*, 2020, 5, 263–269.
- 31 I. R. Baxendale, C. M. Griffiths-Jones, S. V. Ley and G. K. Tranmer, *Synlett*, 2006, 0427–0430.
- 32 H. S. Fogler, *Elements of chemical reaction engineering*, Upper Saddle River, N.J., Prentice Hall PTR, [1999] ©1999, 3rd edn, 1999.

- 33 A. Özdural, A. Alkan-Sungur, I. Boyaci and C. Webb, *Food Bioprod. Process.*, 2008, **86**, 104–108.
- 34 S. Kongjaroon, N. Lawan, D. Trisrivirat and P. Chaiyen, *RSC Chem. Biol.*, 2024, 5(10), 989–1001.
- 35 M. Remko, D. Fitz, R. Broer and B. M. Rode, *J. Mol. Model.*, 2011, **17**, 3117–3128.
- 36 P. De Santis, L.-E. Meyer and S. Kara, *React. Chem. Eng.*, 2020, 5, 2155–2184.
- 37 H. Snyder and F. J. Pilgrim, *J. Am. Chem. Soc.*, 1948, **70**, 3770–3771.
- 38 S. Bunsangiam, N. Thongpae, S. Limtong and N. Srisuk, Sci. Rep., 2021, 11, 13094.
- 39 P. Nutaratat, A. Monprasit and N. Srisuk, *3 Biotech.*, 2017, 7, 1–15.
- 40 N. Menon, D. Richmond, M. R. Rahman and B. R. Menon, *ACS Catal.*, 2022, **12**, 2309–2319.
- 41 H. Kühn and O. Stein, Ber. Dtsch. Chem. Ges. (A and B Series), 1937, 70, 567-569.
- 42 H. M. Gaweska, A. B. Taylor, P. J. Hart and P. F. Fitzpatrick, *Biochemistry*, 2013, 52, 2620–2626.
- 43 B. C. de Andrade, A. Gennari, G. Renard, E. V. Benvenutti, J. M. Chies, G. Volpato and C. F. Volken de Souza, *Catal. Lett.*, 2022, 152, 2956–2970.
- 44 R. L. Hartman, J. P. McMullen and K. F. Jensen, *Angew. Chem., Int. Ed.*, 2011, **50**, 7502–7519.
- 45 J. Kumla, N. Suwannarach, K. Matsui and S. Lumyong, *PLoS One*, 2020, **15**, e0227478.